

---

# Fewshot learning on global multimodal embeddings for earth observation tasks

---

**Matt Allen**

University of Cambridge, UK  
mja78@cam.ac.uk

**Francisco Dorr**

Independent, Argentina  
fran.dorr@gmail.com

**Joseph A. Gallego-Mejía**

Universidad Nacional de Colombia, Colombia  
jagallegom@unal.edu.co

**Laura Martínez-Ferrer**

Universitat de València, Spain  
laura.martinez-ferrer@uv.es

**Anna Jungbluth**

European Space Agency, Climate Office, UK  
anna.jungbluth@esa.int

**Freddie Kalaitzis**

University of Oxford, UK  
freddie.kalaitzis@cs.ox.ac.uk

**Raúl Ramos-Pollán**

Universidad de Antioquia, Colombia  
raul.ramos@udea.edu.co

## Abstract

In this work we pretrain a CLIP/ViT based model using three different modalities of satellite imagery across five AOIs covering over 10% of the earth total landmass, namely Sentinel 2 RGB optical imagery, Sentinel 1 SAR amplitude and Sentinel 1 SAR interferometric coherence. This model uses  $\sim 250$  M parameters. Then, we use the embeddings produced for each modality with a classical machine learning method to attempt different downstream tasks for earth observation related to vegetation, built up surface, croplands and permanent water. We consistently show how we reduce the need for labeled data by 99%, so that with 200-500 randomly selected labeled examples (around 4K-10K km<sup>2</sup>) we reach performance levels analogous to those achieved with the full labeled datasets (about 150K image chips or 3M km<sup>2</sup> in each AOI) on all modalities, AOIs and downstream tasks. This leads us to think that the model has captured significant earth features useful in a wide variety of scenarios. To enhance our model's usability in practice, its architecture allows inference in contexts with missing modalities and even missing channels within each modality. Additionally, we visually show that this embedding space, obtained with no labels, is sensible to the different earth features represented by the labelled datasets we selected.

## 1 Introduction

Earth Observation (EO) has had remarkable progress with the rise of deep learning (DL) methods in the last years and this potential is fueled by the ever increasing availability of satellite imagery [1]. According to the UCS Satellite Database<sup>1</sup>, as of May 2022 there were 470 optical satellites in orbit, 102 radar satellites and 62 tagged as producing some sort of imaging (hyperspectral, multispectral),

---

<sup>1</sup><https://www.ucsusa.org/resources/satellite-database>

among others. Only in ESA’s Sentinel missions, 80 PB of user-level data were downloaded during 2021 [2].

However, it is well known that DL methods are overwhelmingly hungry for labeled data, and one of the main hurdles to effectively exploit DL methods in EO is its endemic scarcity [3]. Even if new EO annotated datasets are published regularly, the time and effort involved cannot keep up with the amount of new data produced by present and future orbiting missions. A number of approaches have been developed to address the labeled data scarcity challenge, including a variety of methods under self supervised learning (SSL) [3], weakly supervised methods [4], among others, more often that not blended into foundation models [5].

CLIP [6] is an SSL method that contrastively learnt how to align the representations of image/text pairs collected from the Internet, allowing to deal with different modalities of the same reality within the same embedding space for a variety multi-modal applications including detection, captioning, VQA and conditional image generation among others. CLIP’s architecture, heavily based on Vision Transformers (ViT) [7], has been applied to merge multimodal representations beyond text and in different domains [8], [9], [10]. CLIP like models are also starting to appear in satellite imagery under different scenarios for temporal and multi-spectral imagery [11], temporal multimodal pixel wise [12] or a multispectral contrastive model for Landsat imagery [13].

In this work we built a three tower CLIP architecture, feed them with Sentinel 2 RGB optical imagery, Sentinel 1 amplitude and Sentinel 1 interferometric coherence, and use the produced embeddings in several downstream classification tasks, representing different earth features. We show how, in this representation space, a small fraction of data is enough to obtain full-dataset level performance reducing by two orders of magnitude the need for labeled data.

This paper is structured as follows. Section 2 describes the Areas of Interest (AOI) used, the input imagery and downstream labels. Section 3 describes the SSL architecture and training procedure, together with the downstream task. Section 4 shows results and visualization and in Section 5 we draw some conclusions.

## 2 Data and downstream tasks

**Input modalities** We use three modalities for input data, taking observations during the first three months of 2020. For each AOI (see below) we built a grid containing tiles (image chips) of size 448m  $\times$  448m. For Sentinel-2 optical data (`s2rgbm`) we use only the three RGB channels which we average per month (thus, 9 channels). For Sentinel-1 amplitude (`s1grdm`) we use the vv and vh polarizations, plus their logarithmic difference, taking also their average per month (thus, 9 channels). Both Sentinel-2 and Sentinel-1 amplitude were tiled from Google Earth Engine using `geetiles`<sup>2</sup> which provides a 10m resolution and thus each chip is 448x448 pixels. We obtained Sentinel-1 interferometric coherence (`gunw`) from ARIA Sentinel-1 Geocoded Unwrapped Interferograms database [14] as available through Alaska’s Satellite Facility<sup>3</sup>, using `sartiles`<sup>4</sup>. Since interferometric coherence is built using pairs of Sentinel-1 observations we selected the pairs available whose second observation was within 2020Q1 and the first one at most 48 days before. Thus, we have a potentially variable number of channels in each tile, depending on the number of interferometric pairs which could be formed. Its resolution is around 90m per pixel, and we upsample the image chips to match the 448x448 pixel size of `s1grdm` and `s2rgbm`.

**Areas of Interest** We defined five AOIs covering regions in Conterminous United States (CONUS, 167K image chips), South America (83K chips), Pakistan and India (Pakin, 147K chips), China (285K chips) and the Middle East (163K chips), as illustrated in Fig. 1. The AOIs extent is determined by the 2020 coverage of the `gunw` dataset. Observe that we do geographical aware splits into train (60%), validation (20%) and test (20%) to avoid as much as possible data leakage from contiguous image chips being in different splits.

**Downstream tasks** We selected four use cases with global labels coverage so that we could experiment on ablations with increasing number of labels available. **Vegetation estimation:** we used

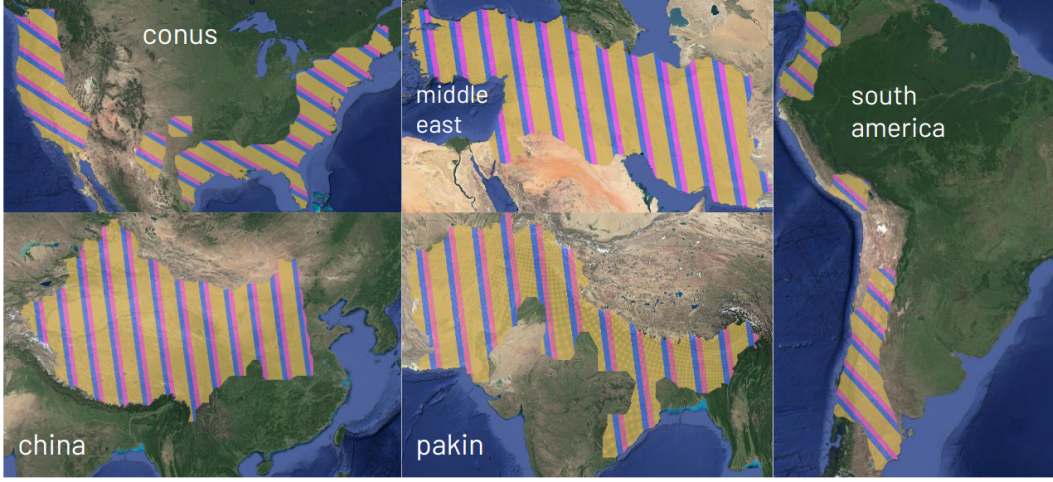
---

<sup>2</sup><https://github.com/rramosp/geetiles>

<sup>3</sup><https://ASF.alaska.edu/data-sets/derived-data-sets/sentinel-1-interferograms/>

<sup>4</sup><https://github.com/rramosp/sartiles>

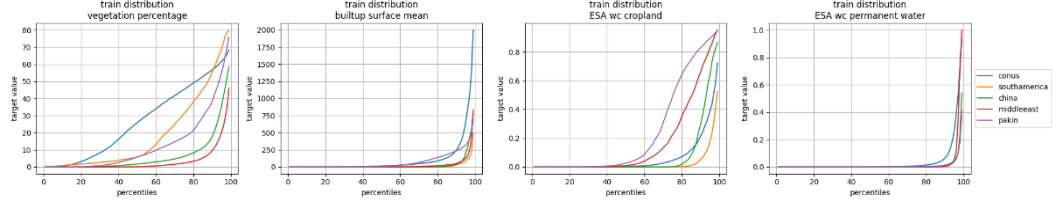
Figure 1: Areas of Interest (AOIs) used in this study. Bands indicate the splits for train (yellow), validation (blue) and test (pink). In total there are 167K image chips for CONUS, 163K chips for Middle East, 147K chips for Pakistan-India, 285K chips for China and 83K chips for South America, which aggregates to 845K chips covering a surface of 16.9M km<sup>2</sup>.



the MOD44B.006 Terra vegetation continuous fields yearly dataset for 2020, focusing on the tree percentage estimation at 250m per pixel<sup>5</sup>. **BuiltUp Surface**, the Global Human Settlement Layer Built-Up surface dataset from the Joint Research Center of the European Commission<sup>6</sup> for 2020 at 100m per pixel. **Croplands**, the ESA World Cover 2020 class representing croplands [15] at a 10m/pixel resolution. **Permanent water**, the ESA World Cover 2020 class representing permanent water bodies [15] at a 10m/pixel resolution. The JRC dataset was downloaded from their site and tiled using `sartiles`, whereas the rest were downloaded and tiled from Google Earth Engine using `geetiles`

For each dataset we define a binary classification task to predict the mean value per chip, thresholded on each AOI so that we get two balanced classes. Within the same task, this threshold is usually different for each AOI as they have different distributions as shown in Fig 2. So, for instance, for `modisveg` we set forth to predict whether an image chip has high or low vegetation, for `ghsbuilt`s we predict whether a chip has high or low built surface, etc.

Figure 2: Distribution of labels on each downstream task and AOI shown as a quantile plot. Observe that most tiles do not contain built surface or permanent waters



### 3 Method

#### 3.1 Model pretraining

We use a Self Supervised Learning approach using Visual Transformers (ViT) and a CLIP based loss architecture, where we have one ViT tower per input modality (`s1grdm`, `s2rgbm` and `gunw`). This architecture produces an embedding for each input image and modality and pushes embeddings of

<sup>5</sup>[https://developers.google.com/earth-engine/datasets/catalog/MODIS\\_006\\_MOD44B](https://developers.google.com/earth-engine/datasets/catalog/MODIS_006_MOD44B)

<sup>6</sup><https://ghsl.jrc.ec.europa.eu/download.php?ds=bu>

different modalities on the same chip to be similar, and others to be different. In practice we are bound to occasional unavailability of particular channels: sometimes vv or vh are not available on Sentinel 1, clouds occasionally hinder Sentinel 2, and the number of interferometric pairs formed for SAR coherence is not always the same. To cope with this, each of the ViT accepts a single channel structure, and we select randomly one single channel of each input modality to feed each ViT at each inference request or training step. Besides enhancing the usability of the pretrained model for downstream tasks to noisy or missing data scenarios, we observed that this setup produces more robust outputs, probably due to the input noise induced by this procedure.

Since we tried different ViT configurations and embedding sizes, we use the train data split for training the model and the validation split to select the best self supervised model according to the CLIP loss. Test data is only used to measure the results presented here. Our final ViT configuration produces an embedding of size 768 for each input image chip in each modality, containing 259M trainable parameters. Train data amounts to about 500K image chips, equivalent to some 10M km<sup>2</sup> and taking about 100 hours of training time on an Nvidia DGX architecture with 8 A100 GPUs, 250 CPU cores and 2TB RAM.

### 3.2 Downstream tasks

For each of the five AOIs and each modality we train a Random Forest to binary classify whether the mean value of each measure (vegetation, built surface, croplands and permanent water) is below or above the median. We use the embeddings representation for each modality as produced by the pretrained model which have a size of 768 components. We create an additional modality by concatenating all three modalities and, thus, produce a vector of size 2304 for each image chip. We do an ablation on the size of the sample taken from the train dataset with 5, 10, 100, 250, 500, 1000, 5000, 20000 and the full dataset. The sample is random uniform across all chips on the training split within each AOI.

We therefore train (3+1) modalities  $\times$  5 AOIs  $\times$  9 train dataset sizes. We use validation data to select the overall best Random Forest configuration (50 estimators and 7 max depth), and then we measure the accuracy on the test data. This is the only time that test data is used. Observe that train data is both used to train the pretrained model and the downstream Random Forest. We repeat this procedure 10 times and report the mean value of each experiment set.

## 4 Results

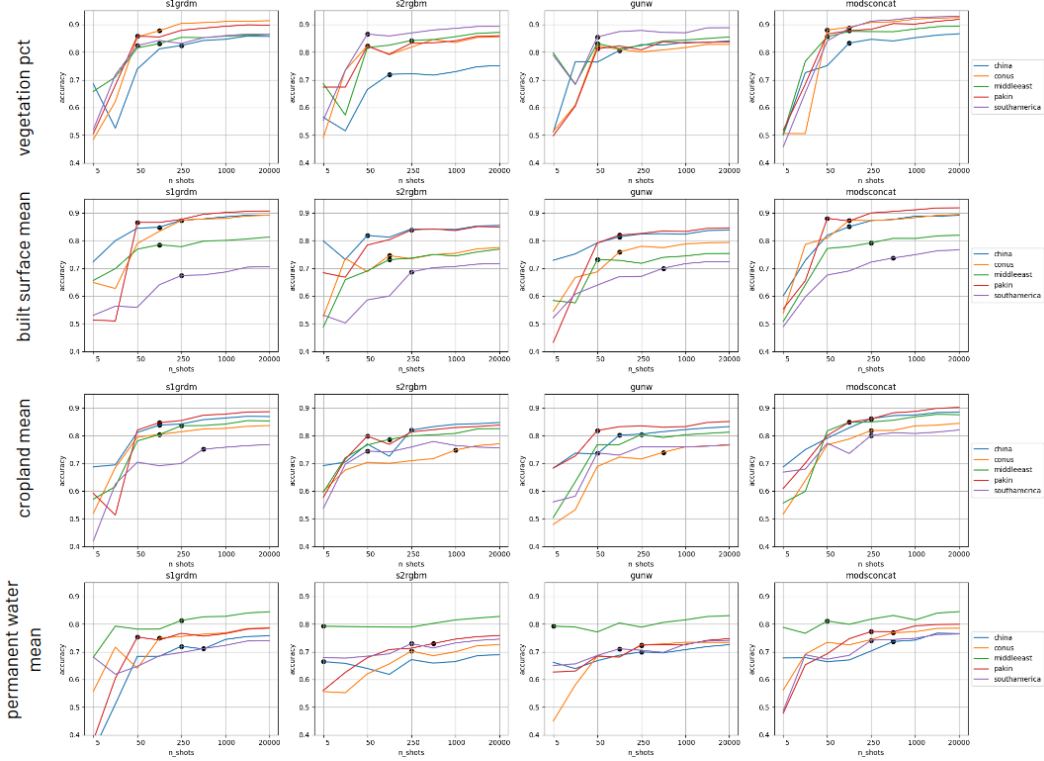
### 4.1 Ablations

Fig. 3 shows the overall accuracy results for our experimentation sets. Recall that we are doing a balanced binary classification task, with a different threshold in each AOI to ensure this balance, thus, reporting accuracy is straightforward. Observe that different tasks have different degrees of difficulty for different modalities. It is interesting to see that, in general, s1grdm embeddings perform better than the rest. Also, concatenating modalities embeddings (modsconcat if Fig. 3) seems to marginally improve overall results. We take as reference the accuracy obtained when using the full dataset, and measure how far we are from it in each experiment. Black dots in Fig. 3 show when the experiment produces an accuracy of at least 95% that of the one obtained with the full labeled dataset. This happens always with less than 500 image chips, and most of the times with less than 250. Considering an average training dataset size of 150K. This means that with only 0.3% of train data (3 per thousand) we can attain 95% of the top performance. The standard deviation was  $<0.05$  with we used 50 or less shots, and  $<0.01$  with larger datasets, so we did not include it in Fig. 3 for clarity.

### 4.2 Embeddings

Finally, Fig. 4 shows a 2D TSNE reduction of the embeddings obtained for each modality (columns), colored by the downstream task log mean value before thresholding for binary classification for each downstream task (rows). Observe that the labels are not used to compute neither the embeddings, nor to the 2D TSNE position. And still we do get clear positional patterns where similar values of the downstream tasks cluster together. We find this significant, as it illustrates how the embeddings do capture terrain features which are useful on different downstream tasks. Although somewhat subtle,

Figure 3: Accuracy on binary classification for each downstream task, AOI and modality. The x-axis is non-linear and represents the number of image chip embeddings used to train a model. Dots signal the minimum number of training image chips which with 95% of top accuracy for each task is achieved. Observe that in the vast majority of cases, with less than 250 labeled image chip we can achieve at least 95% of the accuracy obtained with the full training dataset of labeled images. Training dataset sizes ranges from 50K in South America to 171K in China (60% of the total image chips in each AOI). Accuracy in measured on the full test split (20% of data).



observe as well how, for the same task, different modalities separate clusters value a bit better than others. Fig. 5 shows a couple of example images in the three modalities.

## 5 Conclusion

This work showed the effectiveness of multimodal models pretrained with large amounts of planetary data to reduce the number of required labeled examples in different downstream earth observation classification tasks. The reduction of the required amount of labeled data reaches the orders of 99%. We also run our experiments with smaller pretrained ViT architectures with 11M to 100M parameters and embeddings of size 192 and 364. Although the combined CLIP loss is usually similar to the one obtained with out 250M parameter / 768 encoding size model, the performance of the downstream tasks is degraded, even if it preserves the 95% relative performance as described earlier. This leads us to plan future work with planetary wide datasets and larger models.

## 6 Acknowledgements

This work has been enabled by Frontier Development Lab Europe (<https://fdleurope.org>) a public / private partnership between the European Space Agency (ESA), Trillium Technologies, the University of Oxford and leaders in commercial AI supported by Google Cloud and Nvidia, developing open science for all Humankind.

Figure 4: Embeddings for each AOI and modality projected to a TSNE 2D space for visualization and colored with each downstream task label. Each dot correspond to one image chip projected to this space. These embeddings are trained and computed unsupervisedly with no label information and yet they are sensible to different land features as represented by each downstream task. Scale is logarithmic to better appreciate the value ranges of labels.

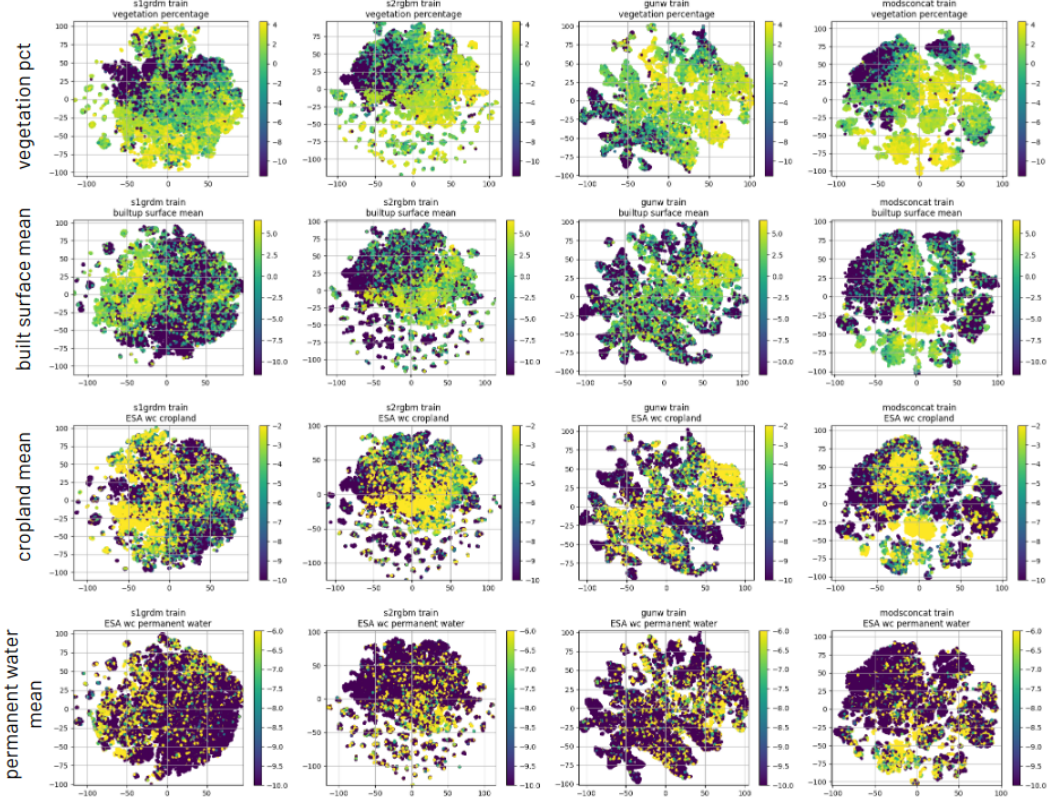
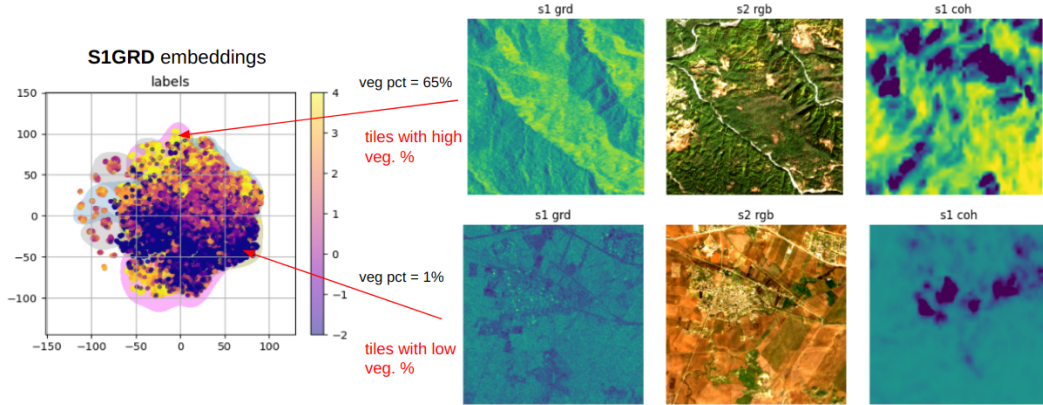


Figure 5: Location in the s1grdm 2D TSNE embedding space for CONUS of two sample image chips with different vegetation percentage value. Different colouring from 4 simply signals a different experimental run.



## References

- [1] Xiao Xiang Zhu, Devis Tuia, Lichao Mou, Gui-Song Xia, Liangpei Zhang, Feng Xu, and Friedrich Fraundorfer. Deep learning in remote sensing: A comprehensive review and list of resources. *IEEE geoscience and remote sensing magazine*, 5(4):8–36, 2017.
- [2] European Space Agency. *Copernicus Sentinel Data Access Annuel Report 2021*. ESA, 2022. URL <https://sentinels.copernicus.eu/web/sentinel/-/copernicus-sentinel-data-access-annual-report-2021>.
- [3] Yi Wang, Conrad M Albrecht, Nassim Ait Ali Braham, Lichao Mou, and Xiao Xiang Zhu. Self-supervised learning in remote sensing: A review. *arXiv preprint arXiv:2206.13188*, 2022.
- [4] Corrado Fasana, Samuele Pasini, Federico Milani, and Piero Fraternali. Weakly supervised object detection for remote sensing images: A survey. *Remote Sensing*, 14(21):5362, 2022.
- [5] Alexandre Lacoste, Evan David Sherwin, Hannah Kerner, Hamed Alemohammad, Björn Lütjens, Jeremy Irvin, David Dao, Alex Chang, Mehmet Gunturkun, Alexandre Drouin, et al. Toward foundation models for earth monitoring: Proposal for a climate change benchmark. *arXiv preprint arXiv:2112.00570*, 2021.
- [6] Alec Radford, Jong Wook Kim, Chris Hallacy, Aditya Ramesh, Gabriel Goh, Sandhini Agarwal, Girish Sastry, Amanda Askell, Pamela Mishkin, Jack Clark, et al. Learning transferable visual models from natural language supervision. In *International conference on machine learning*, pages 8748–8763. PMLR, 2021.
- [7] Alexey Dosovitskiy, Lucas Beyer, Alexander Kolesnikov, Dirk Weissenborn, Xiaohua Zhai, Thomas Unterthiner, Mostafa Dehghani, Matthias Minderer, Georg Heigold, Sylvain Gelly, Jakob Uszkoreit, and Neil Houlsby. An image is worth 16x16 words: Transformers for image recognition at scale, 2021.
- [8] Hongwei Xue, Yuchong Sun, Bei Liu, Jianlong Fu, Ruihua Song, Houqiang Li, and Jiebo Luo. Clip-vip: Adapting pre-trained image-text model to video-language representation alignment. *arXiv preprint arXiv:2209.06430*, 2022.
- [9] Zifeng Wang, Zhenbang Wu, Dinesh Agarwal, and Jimeng Sun. Medclip: Contrastive learning from unpaired medical images and text. *arXiv preprint arXiv:2210.10163*, 2022.
- [10] Junnan Li, Ramprasaath Selvaraju, Akhilesh Gotmare, Shafiq Joty, Caiming Xiong, and Steven Chu Hong Hoi. Align before fuse: Vision and language representation learning with momentum distillation. *Advances in neural information processing systems*, 34:9694–9705, 2021.
- [11] Yezhen Cong, Samar Khanna, Chenlin Meng, Patrick Liu, Erik Rozi, Yutong He, Marshall Burke, David Lobell, and Stefano Ermon. Satmae: Pre-training transformers for temporal and multi-spectral satellite imagery. *Advances in Neural Information Processing Systems*, 35: 197–211, 2022.
- [12] Gabriel Tseng, Ivan Zvonkov, Mirali Purohit, David Rolnick, and Hannah Kerner. Lightweight, pre-trained transformers for remote sensing timeseries. *arXiv preprint arXiv:2304.14065*, 2023.
- [13] Adam J Stewart, Nils Lehmann, Isaac A Corley, Yi Wang, Yi-Chia Chang, Nassim Ait Ali Braham, Shradha Sehgal, Caleb Robinson, and Arindam Banerjee. Ssl4eo-1: Datasets and foundation models for landsat imagery. *arXiv preprint arXiv:2306.09424*, 2023.
- [14] Brett Buzzanga, David PS Bekaert, Ben D Hamlington, and Simran S Sangha. Toward sustained monitoring of subsidence at the coast using insar and gps: An application in hampton roads, virginia. *Geophysical Research Letters*, 47(18):e2020GL090013, 2020.
- [15] Daniele Zanaga, Ruben Van De Kerchove, Wanda De Keersmaecker, Niels Souverijns, Carsten Brockmann, Ralf Quast, Jan Wevers, Alex Grosu, Audrey Paccini, Sylvain Vergnaud, Oliver Cartus, Maurizio Santoro, Steffen Fritz, Ivelina Georgieva, Myroslava Lesiv, Sarah Carter, Martin Herold, Linlin Li, Nandin-Erdene Tsendsazar, Fabrizio Ramoino, and Olivier Arino. Esa worldcover 10 m 2020 v100, October 2021. URL <https://doi.org/10.5281/zenodo.5571936>.